Preparation and Structural Analysis of Carbon-Supported Co Core/Pt Shell Electrocatalysts Using Electroless Deposition Methods

K. D. Beard, David Borrelli, Alison M. Cramer, D. Blom, J. W. Van Zee, and John R. Monnier*

Department of Chemical Engineering, Swearingen Engineering Center, University of South Carolina, Columbia, South Carolina 29208

ABSTRACT Cobalt core/platinum shell nanoparticles were prepared by the electroless deposition (ED) of Pt on carbon-supported cobalt catalyst (Co/C) and verified by HRTEM images. For a 2.0 wt % Co/C core, the ED technique permitted the Pt loading to be adjusted to obtain a series of bimetallic compositions with varying numbers of monolayers (ML). The tendency for corrosion of Co and the electrochemical (*i.e.*, oxygen reduction reaction (ORR)) activity of the structures were measured. The results from temperature-programmed reduction (TPR) analysis suggest that a single Pt ML coverage is formed at a Pt weight loading between 0.5 and 0.7% on the 2.0% Co/C. HRTEM analysis indicates that the continuity of the Pt shell on the Co core depends on the precursor Co particle size, where "large" Co particles (>10 nm) favor noncontinuous, three-dimensional Pt structures and "small" Co particles (<6 nm) favor layer-by-layer growth. For these larger core−shell particles, Co was observed to quickly corrode in 0.3 M H_2SO_4. Surface area specific ORR activity, measured by chemisorption techniques, revealed that the Pt−Co/C catalysts performed better than a commercial Pt/C catalyst; however, on a Pt mass basis, only the lower Pt:Co atomic ratio Pt−Co/C catalysts outperformed the Pt/C catalyst.

KEYWORDS: electroless deposition · platinum · cobalt · core/shell · bimetallic catalyst · oxygen reduction reaction

With the growing attempts to make fuel cell technology economically competitive, much attention has been focused on lowering the cost of the electrocatalysts used for electrochemical reactions. The most common electrocatalyst used in proton exchange membrane fuel cells (PEMFCS) is Pt supported on electrically conductive porous carbon (Pt/C) because it has high activity toward oxygen reduction and it is corrosion-resistant in the acidic environment[1] below 1.2 V. Highly loaded Pt/C catalysts (≥20 wt % Pt) are often used in PEM fuel cells to increase the relatively slow oxygen reduction reaction (ORR)[2−6] and decrease the overpotentials which may approach 0.3 V. Two possible methods to decrease Pt loading are to increase the fraction of surface Pt atoms/total Pt atoms (*i.e.*, increase Pt catalyst dispersion) and to increase the specific activity toward the ORR of the deposited Pt (normalized to Pt surface area).

Many different preparation techniques have been used to increase Pt dispersion by reducing the Pt particle size.[7−13] In some cases,[7−9,11,13] Pt particle sizes have been decreased to less than those of the best commercially available catalysts. Note that the relationship between Pt dispersion and Pt particle size shows that 100% dispersion is achieved at a diameter of approximately 1.1 nm. Therefore, any further reduction in diameter will not increase Pt dispersion.[14] These calculations do not account for the thermodynamic or kinetic stability of such small particles on the surface of carbon, and theoretical and experimental studies of these interactions would be helpful to understand the compromise between dispersion and durability.

On the other hand, several sources have suggested that the specific activity of ORR for very small Pt particles (1−2 nm diameter) is less than that for larger Pt particles (≥4 nm).[3,4,15−22] The origin of the particle size dependency on the kinetics of oxygen reduction has been attributed to higher activity of the Pt(111) and Pt(100) surface planes *versus* corner/edge/defect sites. Van Hardeveld and Hartog[23] have shown that the fraction of corner and edge sites dramatically increases as particle sizes become smaller, which should result in less active catalysts (normalized to active surface area) for ORR.

The other method to decrease Pt loading is to increase the specific ORR activity by combining Pt with another metal in a bimetallic composition. There are many reports of bimetallic Pt−M/C catalysts with increased ORR activity where M is a transition metal such as Fe,[24−27] Ni,[25−33] Co,[25−27,29−32,34−39] or Cu.[26,27,40] The source of

*Address correspondence to monnier@engr.sc.

Received for review March 3, 2009 and accepted July 28, 2009.

Published online August 6, 2009.
10.1021/nn900214g CCC: $40.75

the enhanced oxygen reduction activity has been attributed to a compression of the Pt−Pt bond distance[28,29,34,41−43] and/or an increase in the Pt 3d orbital vacancy,[25,27,30,34,43−46] both of which should make oxygen reduction more facile. Moreover, it has been shown through DFT calculations[47,48] that a weaker Pt−OH bond is the cause of activity enhancement because the adsorbed OH group destabilizes ORR intermediates and blocks adsorption sites. A lower density of states near the Fermi energy level results in a less stable Pt−OH bond. DFT calculations also showed that a decreased Pt−Pt bond distance results in a lower density of energy states at the Fermi level and therefore a destabilized Pt−OH bond. Unfortunately, the highly acidic environment of a PEM fuel cell rapidly corrodes any surface-accessible base metals resulting in leaching of the base metal.[39,49−51]

Another possible method to simultaneously gain an enhancement in oxygen reduction activity, limit corrosion of the base metal, and increase Pt dispersion is to combine Pt with a base metal in a way that creates a structure of the catalyst nanoparticles with a base metal core and a thin Pt shell. In this way, the base metal should be protected from corrosion by the Pt shell. This core/shell structure[52−61] also permits high Pt dispersion regardless of the particle size since the Pt is located only as a shell on the particle surface. If the Pt shell were only one monolayer (ML) thick, then Pt dispersion would be unity regardless of the overall particle diameter (note that the probability of corrosion of a base metal core for such single ML structures has not been explored and may still be large). In addition, another possible advantage of this structure is that high Pt dispersions existing as a shell should also exhibit greater resistance to sintering, a problem that affects very small Pt particles. Last, this structure with a thin Pt shell should permit the surface Pt atoms to interact electronically with the underlying base metal atoms to increase oxygen reduction activity through either a contraction of the Pt−Pt bond distance or greater Pt 3d orbital vacancies.

In this article, we produce nanoparticles with a base metal core/Pt shell structure by using electroless deposition (ED), a catalytic or autocatalytic process whereby a chemical reducing agent reduces a metallic salt onto specific sites of a catalytically active metal.[62] The overall reaction (reaction 1) for electroless deposition is a combination of anodic and cathodic electrochemical partial reactions,[63,64] which are given as reactions 2 and 3, respectively. In the anodic reaction (reaction 2), an aqueous reducing agent (RA) is catalytically activated at the surface of metal M′ to produce electrons (the active reducing species is usually a hydride/chemisorbed H on the surface of metal M′). The electrons then reduce the aqueous reducible metal salt (M^{z+}) on the surface of metal M′ (reaction 3). The overall reaction of electroless deposition is thermodynamically favorable but is kinetically limited by the anodic reaction 2 and is controlled by activation of the reducing agent. Since the deposited metal in reaction 3 is often catalytic for reaction 2, further reduction can occur (autocatalysis), potentially resulting in formation of multiple layers of the reducible metal if reaction conditions permit. Previous studies have shown that there is no deposition of Pt on the catalyst support in the absence of a precursor catalyst; therefore, essentially all supported particles prepared by ED are bimetallic in composition.[8,65−68]

TABLE 1. Effect of Temperature on Final Pt and Co Weight Loadings after ED of Pt on Co/C[a]

temperature(°C)	final Pt wt loading (%)	final Co wt loading (%)
80	4.9	2.5
50	4.3	4.3
25	4.2	6.4

[a]Conditions of experiment: 1:10:5 = $PtCl_6^{2-}$/DMAB/citrate mole ratio; 1/2 of DMAB added at 0 and 20 min. Deposition time = 40 min. Precursor catalyst was 7.0% Co/C prereduced in $NaBH_4$ solution. Theoretical maximum Pt loading = 4.9% (if all $PtCl_6^{2-}$ is deposited).

$$M^{z+}(aq) + RA(aq) \xrightarrow{M'} (M^0 - M') + RA^{z+}(aq) \quad (1)$$

$$RA(aq) \xrightarrow{M'} RA^{z+}(aq) + ze^- \quad (2)$$

$$M^{z+}(aq) + ze^- \rightarrow (M^0 - M') \quad (3)$$

Previously,[8,66] we have used noble metal (Rh or Pd) precursor catalysts for the electroless deposition of Pt to produce smaller Pt-containing bimetallic particles. However, to potentially achieve an increase in oxygen reduction activity and avoid using expensive noble metals as the precursor catalysts, Co is used here as the precursor catalyst. To resist the corrosion of Co, a complete shell of Pt is necessary, but a Pt shell that is too thick will decrease the Pt dispersion and present a Pt surface with catalytic properties no different than bulk Pt. Below we present a methodology for the synthesis of Co core/Pt shell bimetallic catalysts by electroless deposition of Pt on Co; extensive characterization of these particles confirms the formation of a core/shell morphology. These particles are tested for resistance to Co corrosion, and finally, ORR activities are measured and compared to a commercially available Pt/C catalyst.

RESULTS AND DISCUSSION

ED Synthesis Parameters. It was observed that the Co weight loadings of the Pt−Co/C bimetallic compositions prepared by ED of Pt on Co/C were significantly lower than the Co/C loading prior to electroless deposition. To limit this loss of Co during the ED process, the temperature of ED was lowered from 80 to 25 °C. The results presented in Table 1 indicate that, while the temperature of ED had only a small effect on the extent of Pt deposition, final Co weight loading was strongly af-

TABLE 2. Effect of Bath Composition on Erosion of Co in ED Bath[a]

condition of ED bath when liquid sample taken	μg Co in ED bath
$PtCl_6^{2-}$ + citrate + DI-H_2O, pH = 11, T = 80 °C	0
above + 20 min after Co/C added	21
above + 5 min after 1st batch of DMAB added	1027
above + 20 min after 1st batch of DMAB added	1148

[a]Conditions of experiment: 1:10:5 = $PtCl_6^{2-}$/DMAB/citrate mole ratio; 1/2 DMAB added at both 0 and 20 min. Deposition time = 40 min. Temperature of ED = 80 °C; 2500 μg of Co on precursor catalyst when added to ED bath.

fected by temperature. To better understand the mechanism of Co loss, liquid samples were withdrawn from the ED bath at certain intervals and analyzed by atomic absorption to monitor the appearance of Co. The results are given in Table 2. Before the Co/C was added to the solution, there was no Co in the bath; 20 min after the Co/C was added, less than 1% of the Co from the precursor catalyst had leached into the ED bath, indicating there is essentially no corrosion of Co in the ED bath at pH 11 and that Pt does not deposit by displacement deposition (oxidation of Co to reduce $PtCl_6^{2-}$ to Pt^0). Once the DMAB was added to the ED bath, the Co was leached into the ED bath. The Co leaching is likely the result of reduction of Co^{n+} to Co^0 by the DMAB which would remove any electrostatic attraction between Co^{n+} and the support to permit some of the Co^0 to erode into the ED bath.

Core/Shell Structure. HRTEM images were taken of Pt−Co/C samples with high Pt:Co atomic ratios so that if Co core/Pt shell structures were formed, they would be easier to observe by electron microscopy. Sample images of Pt−Co/C are given in Figure 1a−c; there is clearly a darker center in the middle of each particle indicating the presence of a lower atomic weight species, Co in this case. Surrounding the Co core is a brighter shell of Pt (higher atomic weight). For comparison, Figure 1d shows a sample of 20 wt % Pt/XC-72 Vulcan carbon, a commercially available catalyst often used in fuel cell studies. As expected for a monometallic Pt catalyst, there is no contrast in the imaged particle. Further, even though all Pt−Co/C samples were prepared at T = 80 °C, the Pt shell exists in a well-ordered, periodic lattice structure. This indicates that the deposition of Pt occurs in a controlled fashion and not in a spontaneous manner. Usually such order in supported particles is found for samples exposed to much higher temperatures.

While Figure 1 clearly shows that the electroless deposition of Pt on Co/C produces Co core/Pt shell nanoparticles, the observed shells were too thick to give high Pt dispersion and the desired modification of the Pt surface by the Co core. A thinner but still complete Pt shell would give higher Pt dispersion and a greater likelihood of Co−Pt interaction. Because ED methods permit controlled rates and amounts of Pt on precursor surfaces,[65,66] it should be possible to form a thin shell of Pt on the Co core if the surface area of the Co particles can be determined. Unfortunately, H_2 chemisorption, the preferred method for measuring the active surface areas of metal catalysts, cannot be used for Co/C because the Co must be completely reduced to the metallic state prior to H_2 chemisorption. The literature recommends reduction in H_2 at high temperatures (>400 °C) for 4 to 16 h.[69−72] Such high temperatures would almost certainly result in sintering and agglomeration (in addition to possible catalytic reduction of the carbon support to CH_4) and do not represent conditions similar to the reduction of the Co in the ED bath immediately prior to Pt deposition.

To estimate the surface area of the Co particles during electroless deposition, Co particle sizes of different weight loadings of Co/C samples were measured by TEM after *ex situ* reduction in a sodium borohydride bath at room temperature. The Co particle size distributions are shown in Figure 2; a statistically relevant number of particles was counted for each sample. The particle size distributions are all coincidental and show maxima at approximately 5 nm diameter, indicating that increasing the Co weight loading from 0.05 to 0.5 wt % resulted in a greater number of similar-sized Co particles and not Co particle growth. These particle size distributions correspond to an average Co diameter of

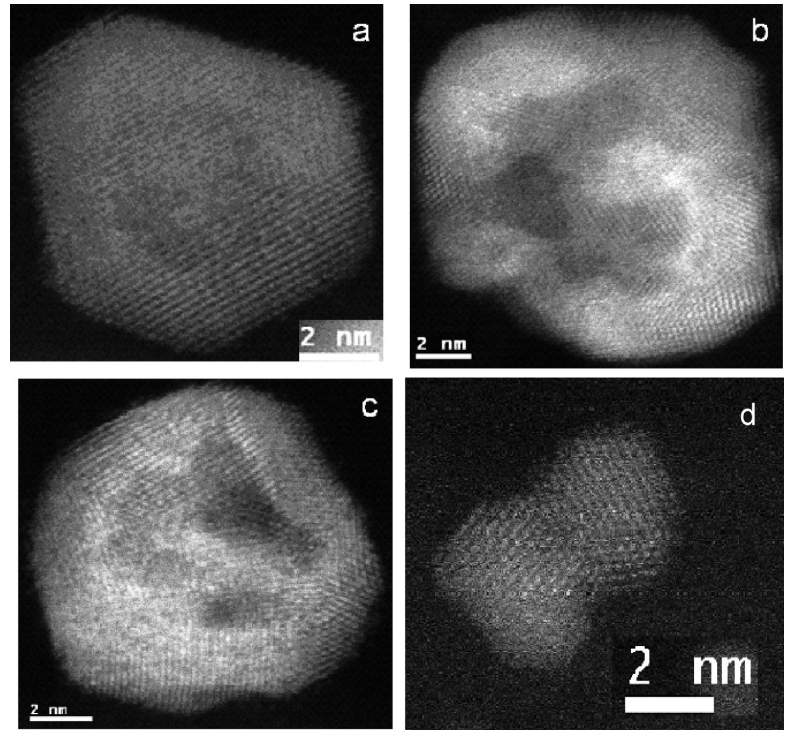

Figure 1. HRTEM images of Pt−Co/C (a−c) samples prepared by the electroless deposition of Pt at 80 °C: (a) 12.5% Pt on 1.0% Co/C; (b) 8.0% Pt on 1.0% Co/C; (c) 4.5% Pt on 1.0% Co/C; and (d) commercial 20% Pt/XC-72 carbon shown for comparison.

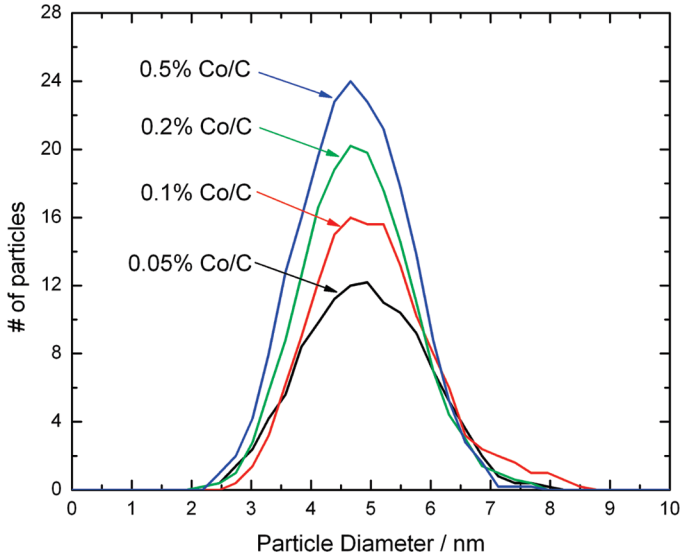

Figure 2. Particle size distribution curves for 0.5, 0.2, 0.1, and 0.05% Co/C. Co particles were observed using TEM and size distributions determined manually. Between 100 and 200 particles were measured for each sample.

approximately 6.0 nm; the active Co surface area, or the area upon which Pt can be electrolessly deposited, is statistically calculated from the particle size distributions. The Co surface area of each different particle size is computed individually and normalized by the fraction of that particle size relative to the total number of particles counted. The total surface area is then determined by summation of all the particle size areas. For a 2.0% Co/C catalyst and assuming monodisperse Pt deposition, approximately 1.1 wt % Pt corresponds to a single Pt monolayer (ML) coverage. This estimate is only approximate and may be higher than the actual amount of Pt actually needed for monolayer coverage since the Co weight loading of 2.0% is greater than those shown in Figure 2 and there may be some particle growth of Co between 0.5 and 2.0% Co. Still, this calculation provides a useful starting point for estimating the amount of Pt necessary for complete encapsulation of the Co core.

To better determine the Pt weight loading and Pt:Co atomic ratio that results in one monolayer of Pt coverage on a 2.0% Co/C sample, a series of Pt−Co/C samples were prepared using the same 2.0% Co/C precursor catalyst; 0.3, 0.5, 0.7, 1.2, and 11.6 wt % Pt were electrolessly deposited to give the corresponding Pt:Co atomic ratios of 0.05, 0.08, 0.11, 0.18, and 1.75, respectively. The Pt−Co/C and Co/C samples were then analyzed by temperature-programmed methods. Prior studies indicated that the differences in temperature of H_2O desorption (as a reaction product) during Pt and Co reduction are large enough to distinguish between the two metals. The H_2O desorption/Pt reduction peak for Pt/C occurs between 25 and 100 °C while that for Co/C is approximately 400 °C. Before temperature-programmed reduction, all samples were pretreated in flowing Ar at elevated temperatures (350 or 425 °C) to remove all physically adsorbed H_2O on the catalyst; after this Ar pretreatment, the appearance of H_2O during TPR can be attributed to Pt or Co reduction. Immediately before the TPR experiments, all samples were pretreated in flowing 2% O_2/balance He by heating the samples at 10 °C/min to 200 °C to ensure surface oxidation of the metallic components. The TPR experiments in 2% H_2/balance Ar are summarized in Figure 3.

Others have shown[72,73] that Pt-assisted reduction of Co lowers the temperature for reduction of Co oxides, which is apparent from the TPR curves in Figure 3. The Co/C monometallic catalyst shows a Co oxide reduction peak centered at approximately 420 °C. After the addition of only 0.3% Pt on 2.0% Co/C, the H_2O peak is shifted to approximately 290 °C due to Pt-assisted, Co oxide reduction. Increasing the Pt weight loading to 0.5% on 2.0% Co/C further reduces the temperature of the H_2O peak to 270 °C, consistent with additional Pt-assisted, Co oxide reduction. Conversely, when the Pt loading is increased to 0.7% Pt on 2.0% Co/C, the H_2O peak shifts to higher temperatures (335 °C), suggesting the presence of diffusional resistance of H_2 to the Co oxide core and/or diffusion of H_2O from the Co core due the existence of a Pt shell. A further increase in temperature of the H_2O peak to 352 °C is observed for 1.2 wt % Pt on 2.0 wt % Co/C, indicating the formation of a thicker Pt shell as more Pt is deposited. When the Pt loading is increased further (11.6% Pt−2.0% Co/C), no H_2O peak is observed, consistent with the formation of a thick Pt shell at these Pt loadings.

The conclusions from Figure 3 suggest that a complete shell of electrolessly deposited Pt is formed on 2.0 wt % Co/C at a Pt weight loading

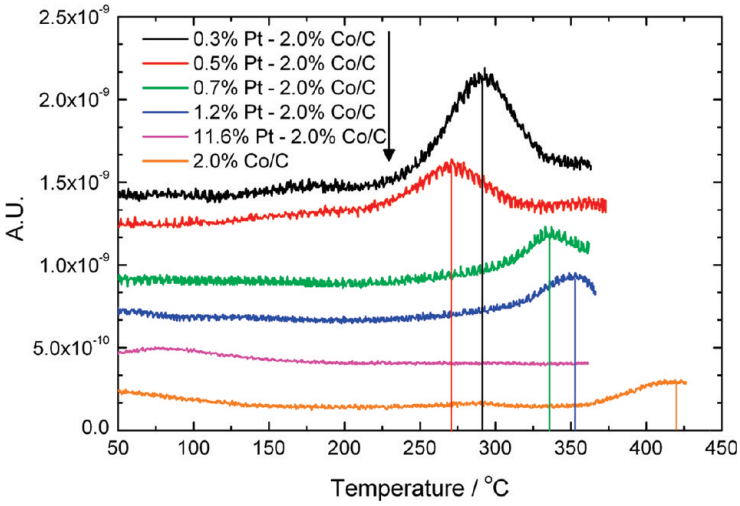

Figure 3. Co reduction/H_2O desorption during temperature-programmed reduction in 2% H_2/balance Ar after oxidation in 2% O_2/He at 200 °C. Samples are (from top to bottom) 0.3% Pt−2.0% Co/C, 0.5% Pt−2.0% Co/C, 0.7% Pt−2.0% Co/C, 1.2% Pt−2.0% Co/C, 11.6% Pt−2.0% Co/C, and 2.0% Co/C. Co reduction/H_2O desorption temperatures are marked on the plots with vertical lines. Pt−Co/C samples were ramped from 30 to 350 °C, and Co/C was ramped from 30 to 425 °C during TPR at rates of 10 °C/min.

between 0.5 and 0.7 wt %. These two samples (0.5 and 0.7 wt % Pt on 2.0 wt % Co/C) were then investigated using HRTEM. Sample images representative of the two samples are shown in Figure 4. The 0.5% Pt−2.0% Co/C (left) sample appears to have only partial Pt coverage; Pt atoms can be clearly identified by the difference in contrast (Pt is brighter). There is much Pt in the center, but Co is seen to be surface-accessible on the perimeter of the particle and spreads out over the carbon surface. Because ED of Pt occurs only on Co sites and not on the carbon support, the outline of the underlying Co particle can be determined by the existence of Pt. Thus, it is obvious there is only a partial Pt shell. The image of 0.7% Pt−2.0% Co/C (right) suggests complete encapsulation of the Co by the Pt; there is no evidence of uncovered Co. The higher loadings of Pt on Co shown in Figure 1 reveal the formation of thicker Pt shells. There appears to be a critical loading of Pt to form complete Pt ML coverage between 0.5 and 0.7 wt % Pt on 2.0% Co/C, which corresponds to a Pt:Co atomic ratio of approximately 0.1. This weight loading is somewhat less than that predicted by estimation of the Co particle size diameter which predicted that ~1.1 wt % Pt would be necessary to completely encapsulate a 2.0% Co/C sample but is certainly within experimental error given the complexity of this system and assumptions made in the calculations of Co surface areas for different Co weight loadings.

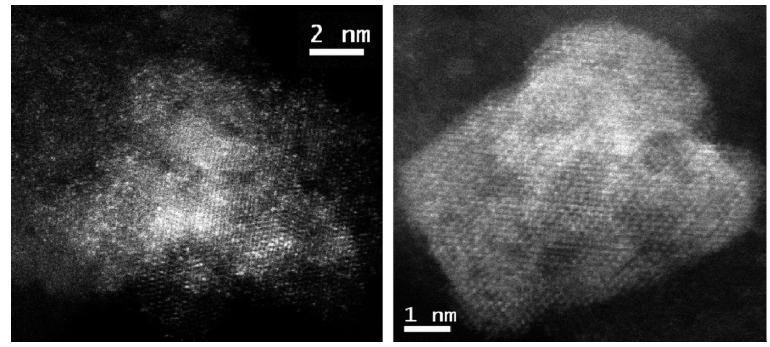

Figure 4. HRTEM images of 0.5% Pt−2.0% Co/C (left) and 0.7% Pt−2.0% Co/C (right) prepared by ED. The 0.5% Pt partially covers the Co as indicated by the bright patches in the middle; however, surface accessible Co remains oxidized and spread out over the carbon surface; 0.7% Pt results in apparent Co coverage by the Pt, and there is no indication of exposed Co on the carbon surface.

Corrosion Characterization. One of the advantages of a core/shell structure is that a complete Pt shell should stabilize a base metal core such as Co from corrosion in an acidic environment. As shown in Figures 1 and 4, ED of sufficient Pt on Co/C should produce bimetallic particles with Pt-encapsulated Co cores. The extent of Co protection by Pt can be determined by immersing the Pt−Co/C compositions in an H_2SO_4 bath, while liquid analysis tracks the extent of Co leaching into the acid bath as a function of time. The results in Figure 5 show the results from a typical corrosion experiment, where the Co from a Co/C precursor catalyst and different Pt−Co/C compositions are leached into the acidic solution. As expected, the Co/C precursor catalyst loses essentially all Co in the first minute. However, substantial fractions of Co are also leached from all of the Pt−Co/C catalysts, with the largest amount of that loss occurring within the first minute. While there is a clear trend that increasing the Pt:Co atomic ratio increases the resistance to Co corrosion, all samples initially have Pt:Co atomic ratios greater than ~0.1 and should have greater resistance to Co corrosion. The extent of corrosion does decrease with increasing Pt coverages, however, indicating that the presence of Pt does lower Co corrosion.

Since nearly all of the corrosion is rapid and occurs in the first minute, it suggests that not all Co/C atoms were encapsulated by Pt. If some of the Co exists as lone atoms or very small particles, they may not be capable of activating the reducing agent (DMAB) that precedes Pt deposition. Earlier work by Lelental[74,75] indicated that a precursor catalyst particle must contain at least two to four (noble metal) atoms to activate DMAB. To test the possibility that some of the Co particles were subcritical in size for Pt deposition, a Co/C precursor catalyst, normally prereduced in a $NaBH_4$ bath at room temperature, was prereduced in H_2 at 400 °C for 2 h to effect sintering of Co to form larger particles. Roughly equal masses of Pt were then electrolessly deposited on the $NaBH_4$-reduced and the H_2-reduced Co/C precursor catalysts. These different Co/C and Pt−Co/C

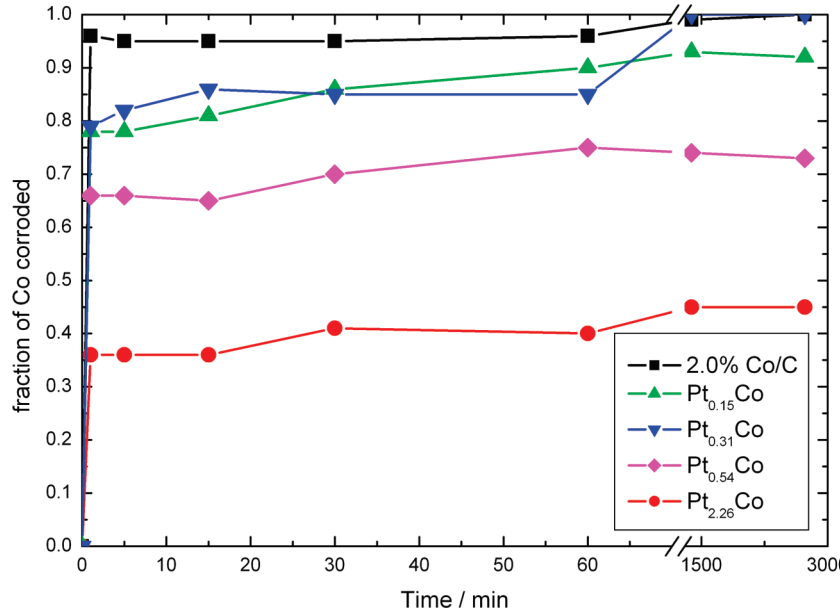

Figure 5. Fraction of Co leached from Pt−Co/C and Co/C samples in 0.3 M H_2SO_4 solution that was deaerated with bubbling N_2 before leaching experiments.

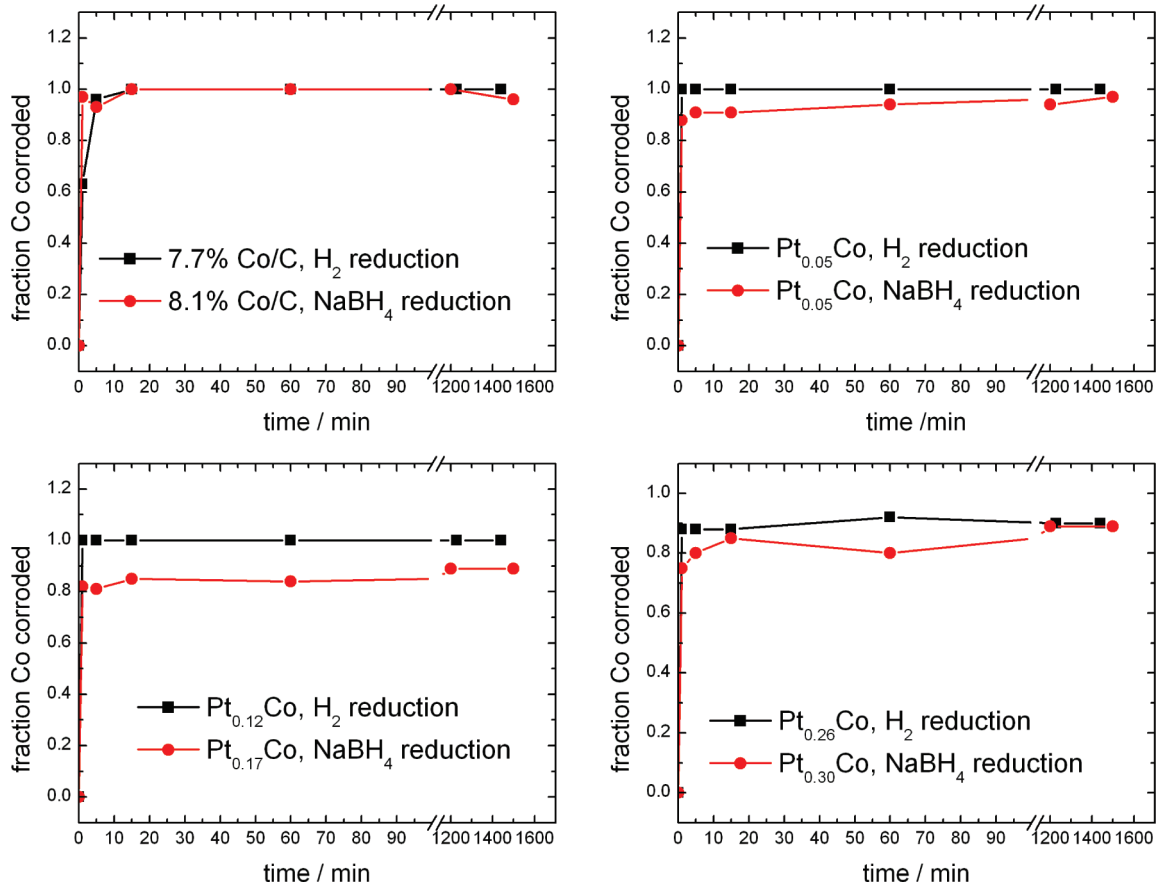

Figure 6. Effect of Co reduction methods on fraction of Co leached in 0.3 M H_2SO_4 solution that was deaerated with bubbling N_2 before leaching experiments. The Co/C catalysts were prereduced in $NaBH_4$ at room temperature or in H_2 at 400 °C (top left) and subjected to ED of Pt to form Pt:Co atomic ratios of 0.05 (top right), 0.15 (bottom left), and 0.30 (bottom right).

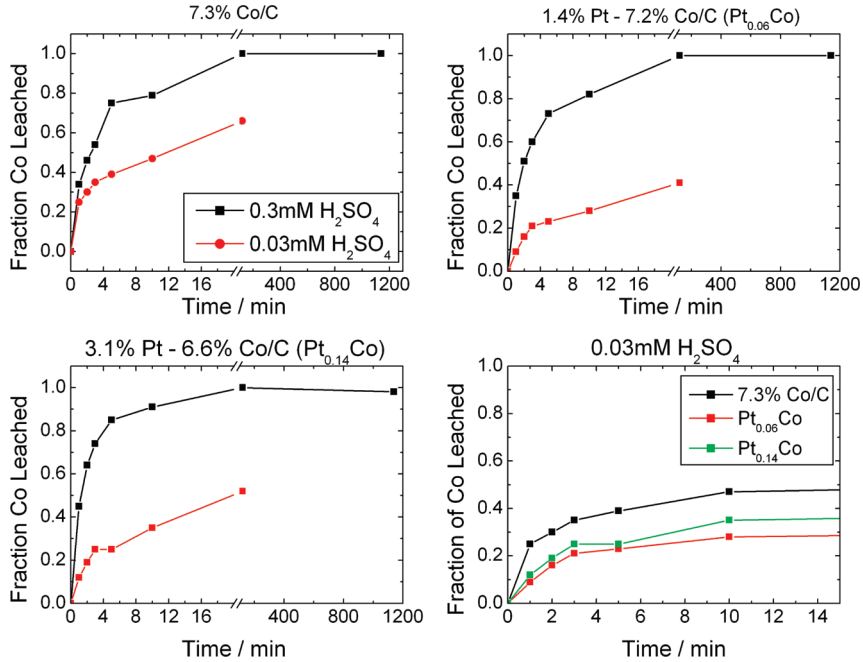

Figure 7. Effect of electrolessly deposited Pt on the rate of Co leaching from Pt−Co/C in 0.3 and 0.03 mM H_2SO_4. Co is leached from a 7.3% Co/C ($NaBH_4$-reduced) precursor catalyst (top left), 1.4% Pt−7.2% Co/C (Pt:Co atomic ratio = 0.06, top right), and 3.1% Pt−6.6% Co/C (Pt:Co atomic ratio = 0.14, bottom left). A comparison of the rates of Co leaching for 0.03 mM H_2SO_4 is given in the bottom right.

catalysts were subjected to the same corrosion test as used for Figure 5, and the results are given in Figure 6. Both the H_2- and $NaBH_4$-reduced Co/C samples exhibited very high extents of corrosion in the first minute, although, as expected, the higher loadings of Pt gave lower levels of Co corrosion. Surprisingly, the Pt−Co/C catalysts prepared from the H_2-reduced Co/C samples had less resistance to Co corrosion than the analogous catalysts prepared by $NaBH_4$-reduced Co/C. The high temperature reduction in H_2 did form very large Co particles as corroborated by HRTEM, so subcritically sized Co particles unable to activate DMAB are not responsible for the Co corrosion in Figure 5. Further, the larger Co particles formed by H_2 reduction have less surface area compared to the Co particles formed by $NaBH_4$ reduction, so the Pt shells should be thicker for the H_2-reduced Co particles. The corrosion results in Figure 6 are not consistent with this hypothesis.

To determine whether the deposited Pt lowered the rates of Co corrosion within the first minute, a more dilute H_2SO_4 solution was used. The 0.3 M H_2SO_4 solution was diluted by factors of 10^3 and 10^4 to 0.3 and 0.03 mM concentrations, respectively, and the results are given in Figure 7 for the Co/C precursor sample and different coverages of Pt on Co/C (same samples as in Figure 6). As expected, the rates of Co leaching were lower for the 0.03 and 0.3 mM H_2SO_4 solutions. When Co leaching rates for the different samples are compared for 0.03 mM H_2SO_4, it is clear that the presence of the Pt does restrict the rate of Co loss compared to the Co/C precursor catalyst. However, the difference in rates of Co leaching for the two Pt−Co/C samples is quite small and implies a mechanism of Pt growth that is not layer-by-layer encapsulation of Co.

Several contradictions arise from the corrosion data in Figures 5−7 and the HRTEM images presented in Figures 1 and 4. The thicker Pt shells deposited on H_2-reduced Co/C do not result in improved Co resistance to corrosion, but actually result in more Co leaching than for the thinner Pt shells deposited on $NaBH_4$-reduced Co/C. Further, while the presence of Pt on Co/C does lower the rate of Co leaching, additional deposition of more Pt does not appreciably increase the resistance of the Co to corrosion, although the much higher Pt loadings present in $Pt_{0.54}Co$ and $Pt_{2.26}Co$ samples (Figure 5) do substantially suppress Co leaching. To resolve these conflicts, the structures of several Pt−Co/C catalysts were further examined with HRTEM. Figure 8 presents a compilation of several different Pt−Co/C catalysts prepared by electroless deposition of Pt at room temperature. Figure 8a−d shows images of different particles from 1.2% Pt−7.6% Co/C ($NaBH_4$ reduced) which correspond to a Pt:Co atomic ratio of 0.05. From the data in Figure 3, a Pt:Co atomic ratio of 0.05 should form slightly less than 1 ML of Pt coverage on the Co/C precursor catalyst, assuming the Co particle sizes for 7.6% Co/C are not appreciably different than those for 2% Co/C. In Figure 8a,b, Pt appears to be deposited as a partial shell over the Co core. However, Figure 8c,d, which shows larger Co particles from the same sample, indicates that Pt is deposited as three-dimensional aggregates on the Co surface. Figure 8e,f shows two different particles from a sample containing 4.8% Pt−5.6% Co/C ($NaBH_4$-reduced) that has a much higher Pt:Co atomic ratio of 0.26. The particle in Figure 8e shows complete encapsulation of the Co core by a Pt shell, suggesting layered Pt deposition; conversely, Figure 8f shows extensive Pt aggregation on the Co core. These images represent a consistent trend observed with other HRTEM micrographs in which "small" Co particles (≤6 nm) result in Pt shell formation, while "large" Co particles (≥10 nm) favor the formation of Pt aggregates on the Co surface. This marked difference in appearance of Pt−Co particles suggests the mechanism of Pt deposition is dependent on Co particle size.

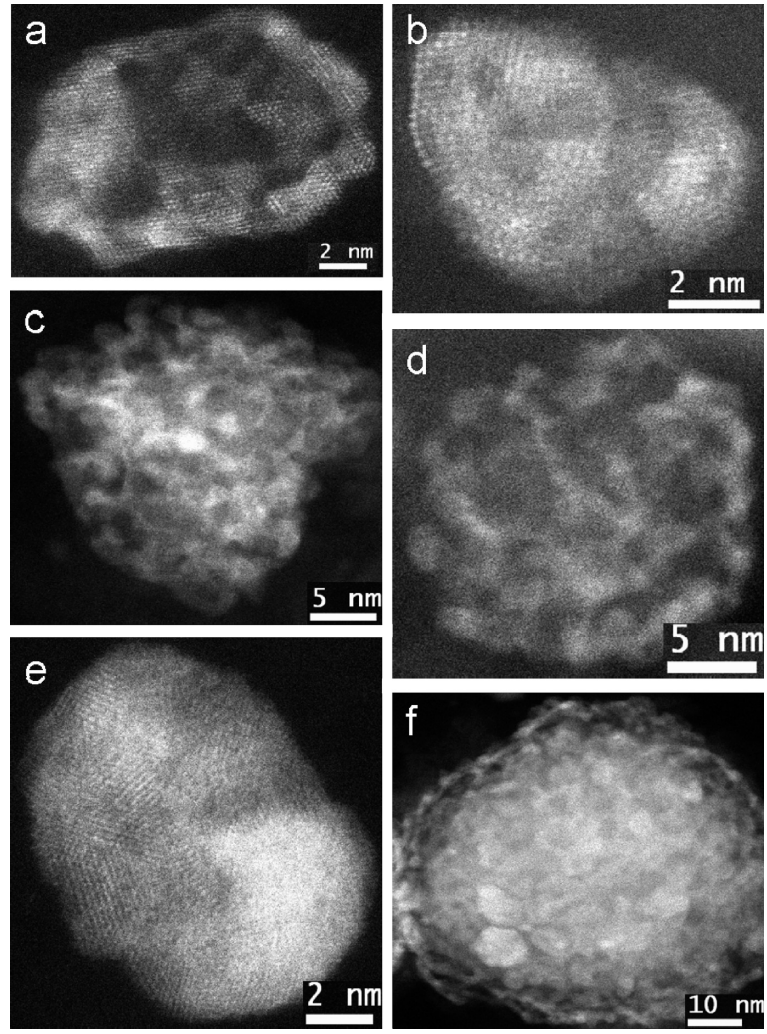

Figure 8. HRTEM images of 1.2% Pt−7.6% Co/C (a−d) and 4.8% Pt−5.6% Co/C (e,f) prepared by ED of Pt at room temperature. The partial shell coverage of small Co particles by Pt in (a) and (b) contrasts with the three-dimensional Pt aggregates on the larger Co particles in (c) and (d). (e) Complete encapsulation of a smaller Co particle compared to extensive Pt aggregation on a larger Co particle in (f).

There are two potential reasons why larger Co precursor particles favor deposition of Pt as aggregates, rather than as a shell. First, the "large" Co particles may be just an agglomeration of smaller particles creating an irregular surface which makes it very difficult to deposit Pt as a layer. Second, if the "large" Co particles are actually large single particles and not an agglomeration of smaller particles, the surfaces would more closely resemble that of a Co single-crystal surface. Much of the Pt−Co work to date has focused on vapor deposition of Pt on Co single-crystal surfaces such as Co(0001), which has been found to favor formation of Pt aggregates.[76−79]

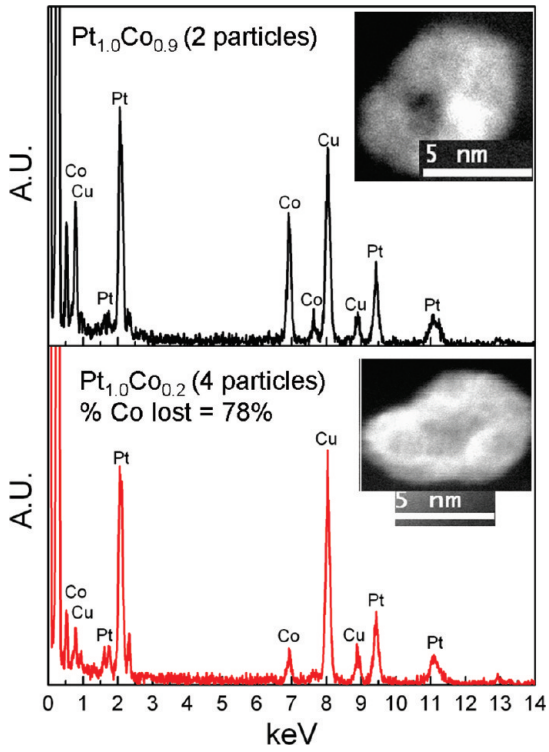

Figure 9. EDX spectra and HRTEM images for small Pt−Co/C particle from 1.2% Pt−7.6% Co/C before (top) and after (bottom) acid treatment in 0.3 M H_2SO_4. The Pt:Co atomic ratio changes from 1.0:0.9 to 1.0:0.2, a loss of 77% of the Co.

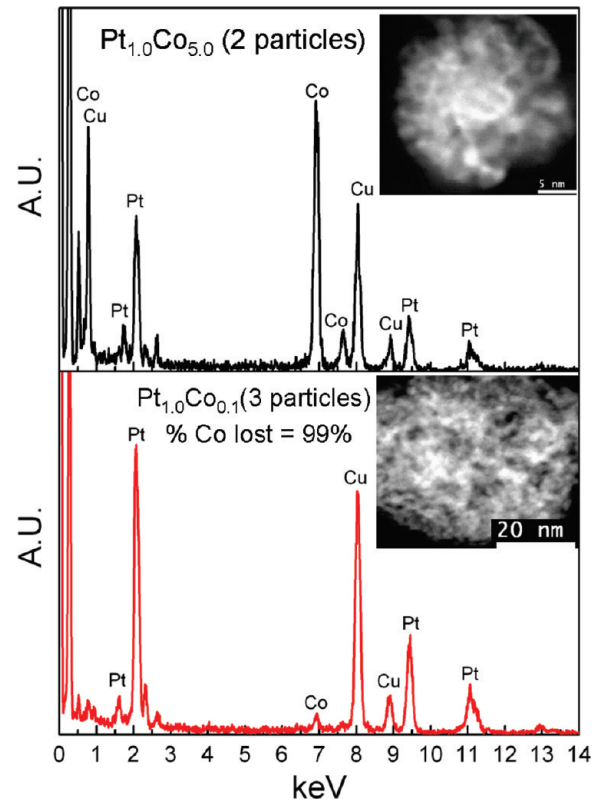

Figure 10. EDX spectra and HRTEM images for large Pt−Co/C particle from 1.2% Pt−7.6% Co/C before (top) and after (bottom) acid treatment in 0.3 M H_2SO_4. Pt:Co atomic ratio changes from 1.0:5.0 to 1.0:0.1, a loss of 99% of the Co.

Because the structure of Pt−Co particles appears to change with Co precursor particle size, it is necessary to measure the effect of acid treatment on different-sized particles instead of the catalyst as a whole. To determine the atomic composition of individual Pt−Co particles both before and after Co leaching in 0.3 M H_2SO_4 for 1 h, small and large Pt−Co particles from a 1.2% Pt−7.6% Co/C catalyst (Pt:Co atomic ratio = 0.05) were imaged with HRTEM and the atomic compositions were determined by energy dispersive X-ray (EDX) analysis. These results are presented in Figures 9 and 10 for a small Pt−Co/C particle and a large Pt−Co/C particle, respectively. Only one EDX spectrum and HRTEM image are shown for each particle size before and after acid treatment; however, the calculated composition which is included in the figure represents an average of several such particles that were analyzed. The stoichiometry of the sample prior to acid treatment is found at the top of each figure, while after acid treatment, the stoichiometry is shown at the bottom. Integration of the Co and Pt peak areas provides an atomic composition for a given particle. This calculation is performed by the EDX control program (INCA software) and includes a calculation of the theoretical relative X-ray emission efficiencies of Pt and Co to make a more accurate estimate of the particle composition in Table 3. Note that in Table 3 and Figures 9 and 10 we show atomic compositions as $Pt_{1.0}Co_x$ to more easily compare compositions before and after acid treatment since Pt is not leached during acid treatment (confirmed by AA analysis).

For the small Pt−Co particle before acid treatment (top of Figure 9), both Co and Pt peaks are clearly identifiable to give a calculated estimate of $Pt_{1.0}Co_{0.9}$ composition for this small particle. After corrosion of Co (bottom of Figure 9), the Co peaks are much smaller than the Pt and Cu (from the Cu grid on which the sample was placed) peaks, indicating loss of Co; the calculated composition is $Pt_{1.0}Co_{0.2}$ representing a 78% loss of Co. By comparison, the fraction of Co leached from the large Pt−Co particle is much greater, as shown in Figure 10. In Figure 10, the Co peak before acid treatment is larger than the Pt and Cu peaks; however, after acid treatment, the Co peaks are barely observed. Further, the calculated composition drops from $Pt_{1.0}Co_{5.0}$ (before acid) to $Pt_{1.0}Co_{0.1}$ (after acid), a loss of 99% of the Co, a

TABLE 3. Composition of 1.2% Pt−7.6% Co/C (Bulk Composition) as a Function of Co Particle Size Prior to and after Immersion in 0.3 M H_2SO_4 for 1 h

particle	Co:Pt atomic ratio ($Pt_{1.0}Co_x$)	% Co lost after acid treatment
small,[a] before H_2SO_4	0.9:1	n/a
small,[a] after H_2SO_4	0.2:1	77
large,[b] before H_2SO_4	5.0:1	n/a
large,[b] after H_2SO_4	0.1:1	99

[a]Small particle ≲6 nm. [b]Large particle ≳10 nm.

much greater compositional change than observed for the small Pt−Co particle. This result supports a growth mechanism of Pt aggregates on larger Co particles and layered deposition of Pt to form shells on smaller Co particles. This results in at least partial encapsulation by Pt of the smaller Co particles, while the larger Co particles are not adequately protected by the Pt against corrosion. However, even the strongly implied existence of Pt shells over a Co core does not completely protect the Co core from corrosion, indicating further work is needed to prepare optimal compositions of Pt shell/Co core particles. The relatively uneven and poor control over Co particle sizes also indicates that much work remains to be done to determine the factors that affect Co particle formation. For this bimetallic system, the electroless deposition of Pt appears to be better understood than Co particle formation.

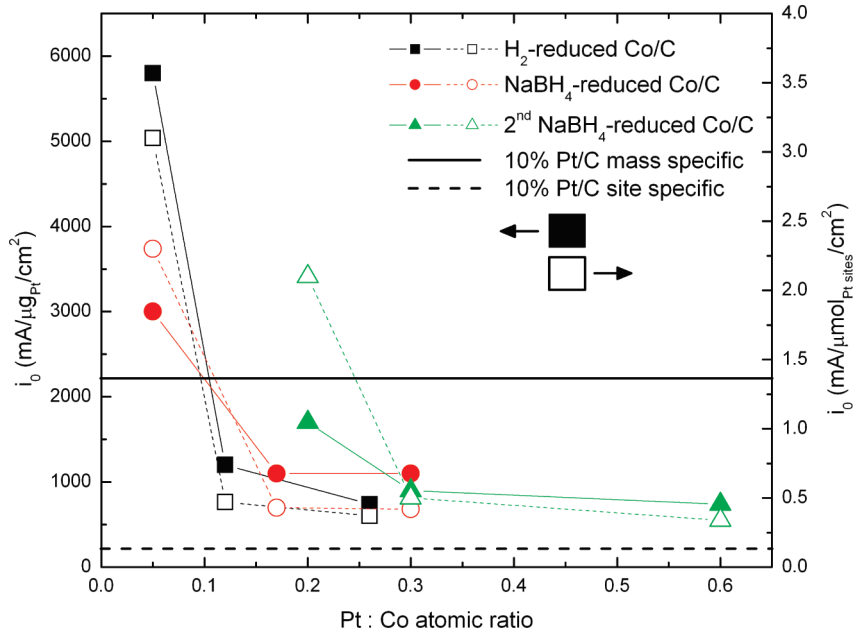

Figure 11. Exchange current densities of Pt−Co/C and Pt/C catalysts expressed as a function of the Pt:Co atomic ratio (Pt/C data represented by horizontal lines). Exchange current densities are normalized to the mass of Pt (left axis, filled markers, solid lines) and the number of surface sites (right axis, hollow markers, dotted lines) as measured by H chemisorption.

ORR Activity Characterization. The ORR activity of several Pt−Co/C catalysts was determined and compared to a commercially available E-tek Pt/C catalyst using a rotating disk electrode (RDE). The electrolyte was saturated with O_2 prior to each recorded polarization curve; six polarization curves were taken for each catalyst film, all at 1000 rpm. Tafel regions in the polarization curves, identified by the linear section from a plot of overpotential *versus* ln i_k, were analyzed to determine the Tafel slope, the exchange current density, and the cathodic transfer coefficient. The Tafel region was between approximately −0.1 and −0.2 V of overpotential, while mass transfer effects became apparent at overpotentials less than −0.3 V. Overpotentials were calculated by subtracting the open circuit voltage of the cathode relative to the reference electrode at the beginning of each experiment from the voltage at a particular current during the experiment measured relative to the reference electrode. The calculations to determine the kinetic coefficients can be found in the literature.[80] The calculated exchange current density (i_0), an excellent tool to compare the relative activities of different electrocatalysts, is given in Figure 11 as a function of the Pt:Co atomic ratio (the commercial Pt/C data are represented by horizontal lines). The exchange current density is normalized to both the Pt mass (left axis) and the Pt surface area (right axis), which was determined by H_2 chemisorption. The TPR data presented in Figure 3 indicate that O precovered Co will not reduce at temperatures less than 225 °C. Thus, pulsing H_2 over the O precovered Pt−Co/C catalysts at ambient temperature will titrate only the Pt surface sites and not Co, permitting determination of the Pt surface area.

Three different groups of Pt−Co/C catalysts were tested: three Pt−Co/C samples prepared from H_2-reduced Co/C (Co corrosion tested in Figure 6), three Pt−Co/C samples prepared from $NaBH_4$-reduced Co/C (Co corrosion tested in Figure 6), and a second set of Pt−Co/C samples prepared from a different $NaBH_4$-reduced precursor catalyst. Previous work indicated that the 0.1 M $HClO_4$ electrolyte used in the RDE experiments leached Co as effectively as the 0.3 M H_2SO_4 acid used in the corrosion experiments. Therefore, the kinetic data reported in Figure 11 take into account the initial loss of Co that was observed in Figure 6. For all three sets of Pt−Co/C samples, the highest ORR activity was achieved at the lowest Pt:Co atomic ratio, indicating that the sample with the thinnest Pt shell yields the greatest activity enhancement. On a Pt mass basis, only those Pt−Co/C catalysts with the lowest Pt:Co atomic ratios for the H_2-reduced and $NaBH_4$-reduced Co/C groups have ORR activities higher than that for the commercially available Pt/C catalyst. Conversely, on a Pt surface area basis, all Pt−Co/C samples exhibit higher ORR activities than the E-tek Pt/C catalyst. Since most of the Co has already been corroded when these measurements were taken, the small fraction of remaining Co must cause the ORR activity enhancements and be fully encapsulated by a Pt shell (otherwise it would be fully corroded). Last, it is interesting to note that the Pt site specific i_0 values for the catalysts prepared with $NaBH_4$-reduced Co/C are relatively greater than the

mass specific i_0 and that this trend is reversed for the catalysts prepared with H_2-reduced Co/C. This observation underscores the effect that large Co particles (a greater fraction of which are present in the H_2-reduced Co/C than the $NaBH_4$-reduced Co/C) result in three-dimensional Pt growth (which have no activity enhancement after Co leaching), while small Co particles encourage layer-by-layer Pt deposition at room temperature (and would maintain an activity enhancement after Co corrosion).

METHODS

Catalyst Synthesis. Using the general procedure of previous work,[8,66] Vulcan XC-72 (254 m^2/g[81]) from Cabot Corporation was cleaned and oxidized in 5 M HNO_3 for 2 h at 50 °C and then rinsed with deionized water (DI-H_2O) and dried under vacuum. This oxidative treatment forms carboxylic acid (RCOOH) groups on the carbon surface. The carbon was then treated at 50 °C in a pH 14 bath for 60 min to deprotonate the carboxylic acid groups to form the corresponding carboxylate ($RCOO^-$) surface species, which electrostatically interact with cationic metal salts to form more highly dispersed metal precursor catalysts (after a reduction treatment) as demonstrated previously.[66] Cobalt was impregnated on the support by dissolving an appropriate quantity of $CoCl_2$ in approximately 20 mL of ethanol and then slurrying with the pretreated carbon support. Excess solvent was removed by rotary evaporation at 65 °C under vacuum. The Co was then reduced by either room temperature exposure to an aqueous sodium borohydride bath (molar ratio of $BH_4^-/Co^{2+} > 10$) or in flowing H_2 at 400 °C in a tubular reactor. Platinum was electrolessly deposited on the cobalt using an ED bath containing H_2PtCl_6, dimethylamine borane (DMAB), and sodium citrate, where DMAB is the chemical reducing agent and sodium citrate is the stabilizing agent. All electroless deposition baths were composed of a 1:10:5 molar ratio of Pt/DMAB/citrate at an initial pH of 11; half of the DMAB was added initially and the remaining DMAB added 20 min later. Deposition times were kept constant at 40 min, and the temperature was maintained at 80 °C, 60 °C, or ambient temperature; previous work had indicated that deposition of Pt was essentially complete after 30 min.

Characterization Methods. Percent weight loadings of Pt and Co (defined as $100 \times g_{metal}/g_{catalyst}$) were determined by atomic absorption (Perkin-Elmer 3300 spectrometer) using conventional analysis protocols. HRTEM images were taken with a JEOL JEM 2100F 200 kV FEG-STEM/TEM equipped with a CEOS C corrector on the illumination system. Geometrical aberrations were measured and controlled to provide less than a $\pi/4$ phase shift of the incoming electron wave over the probe-defining aperture of 15.4 mrad. High angle, annular dark-field (HAADF) STEM images were acquired on a Fischione Model 3000 HAADF detector with a camera length such that the inner cutoff angle of the detector was 50 mrad. The scanning acquisition was synchronized to the 60 Hz ac electrical power to minimize 60 Hz noise in the images; finally, a pixel dwell time of 32 μs was selected.

Temperature-programmed reduction studies were conducted using approximately 50 mg of powdered sample that was loaded into a miniature Pyrex or quartz reactor that was placed in a custom, split tube furnace capable of being heated at linear rates from 2 to 50 °C/min. Sample temperatures were measured by a thermocouple embedded in the catalyst bed. All gases were supplied by National Welders and passed through H_2O and O_2 scrubbers (with the exception of the 10% O_2/He gas mixture which was passed through only the H_2O scrubber) supplied by Restek. Gas flow rates over the samples were controlled with Brooks mass flow controllers, and an MDC variable leak valve was used to adjust gas leak rates into an Inficon Transpector 2 residual gas analyzer. Mass intensity data for the gases of interest and sample temperature were collected and stored in a dedicated computer. Before TPR analysis, all samples were pretreated in flowing Ar at elevated temperatures, 350 °C for bimetallic Pt−Co/C and 425 °C for Co/C samples, to remove physically bound H_2O. The samples were then cooled to 30 °C in flowing Ar, and the gas flow changed to 2% O_2/balance He (50 sccm). Samples were ramped to 200 at 10 °C/min before cooling to ambient temperature. The purpose of this step was to ensure oxygen coverage of the Pt and Co surfaces before temperature-programmed reduction. After flushing in flowing Ar, TPR experiments (10 °C/min) in 2% H_2/balance Ar (50 sccm) were conducted.

For corrosion experiments, 0.01 g of the Co/C precursor catalyst or the ED Pt−Co/C catalyst was immersed in 150 mL of 0.3 M, 0.3 mM, or 0.03 mM H_2SO_4 solutions. The acidic solution was deaerated prior to and during all experiments by bubbling N_2 to remove any interference from the oxygen electrode on corrosion of the Co by the hydrogen electrode. Liquid samples were withdrawn from the solution at different time intervals and passed through a 0.2 μm pore filter to remove any solids. The Co concentration of the samples was measured by atomic absorption (Perkin-Elmer atomic absorption spectrometer 3300) using conventional analysis protocols. After the corrosion experiments were completed, the samples were filtered, washed repeatedly, and dried under vacuum.

Electrochemical characterization was conducted using a glassy carbon, rotating disk electrode (RDE) with a surface area of 0.287 cm^2 attached to a Pine Instruments AFASR rotator and a Princeton Applied Research PAR-283 potentiostat. Catalyst films were deposited on the RDE from sonicated aliquots of a suspension containing 5 mg catalyst/mL solution (1:1 volume ratio of H_2O/isopropyl alcohol) to give a film containing 5 μg of Pt per film. The catalyst films were fixed to the RDE with aliquots of a Nafion solution (1:20 isopropyl alcohol/Nafion) such that the ratio between the volume of Nafion solution and the mass of catalyst in the film was always 0.1 μL/μg catalyst. This was to ensure that all reported ORR activities were not affected by different O_2 diffusional resistances caused by the Nafion, which was shown to have an order of magnitude effect on ORR activity. Three replicate films for each sample were used to obtain the kinetic data. A standard calomel electrode, isolated from the system by a Luggin capillary, was used as the reference electrode, and voltages were reported relative to the standard hydrogen electrode (SHE). The counter electrode was a Pt wire which was also isolated by enclosure in a glass tube with a fritted tip. The electrolyte (0.1 M $HClO_4$) was saturated with O_2 prior to measuring polarization curves that were taken at 5 mV/s at a rotation speed of 1000 rpm. All ORR measurements were taken at ambient temperature.

To normalize the ORR activity to the Pt surface area, the Pt site concentrations for the Pt−Co/C and Pt/C samples were determined by H_2 chemisorption using a Micromeritics AutoChem 2920 chemisorption analyzer. The Pt component (but not the Co) was readily reduced in H_2 at 150 °C before being exposed at 25 °C to O_2 from a flowing 10% O_2/90% He gas stream. Hydrogen was then pulsed over the oxygen precovered Pt surface, and uptake of H_2 was measured by a thermal conductivity detector. The number of Pt surface sites was determined using a stoichiometry of 1 Pt atom−3/2 H_2 molecules according to reaction 4 given below.

$$\frac{3}{2}H_2 + Pt{-}O \rightarrow Pt{-}H + H_2O \quad (4)$$

Acknowledgment. The authors gratefully acknowledge the NSF for funding this work through the IUCRC for fuel cell research supplement award (Grant No. EEC-0324260).

REFERENCES AND NOTES

1. Li, X.; Huang, Q.; Zou, Z.; Xia, B.; Yang, H. Low Temperature Preparation of Carbon-Supported Pt−Co Alloy Electrocatalysts for Methanol-Tolerant Oxygen Reduction Reaction. *Electrochim. Acta* **2008**, *53*, 6662–6667.

2. Bezerra, C. W. B.; Zhang, L.; Lee, K.; Liu, H.; Marques, A. L. B.; Marques, E. P.; Wang, H.; Zhang, J. A Review of Fe-N/C and Co-N/C Catalysts for the Oxygen Reduction Reaction. *Electrochim. Acta* **2008**, *53*, 4937–4951.
3. Bezerra, C. W. B.; Zhang, L.; Liu, H.; Lee, K.; Marques, A. L. B.; Marques, E. P.; Wang, H.; Zhang, J. a Review of Heat-Treatment Effects on Activity and Stability of PEM Fuel Cell Catalysts for Oxygen Reduction Reaction. *J. Power Sources* **2007**, *173*, 891–908.
4. Mayrhofer, K. J. J.; Strmcnik, D.; Blizanac, B. B.; Stamenkovic, V.; Arenz, M.; Markovic, N. M. Measurement of Oxygen Reduction Activities *via* the Rotating Disc Electrode Method: From Pt Model Surfaces to Carbon-Supported High Surface Area Catalysts. *Electrochim. Acta* **2008**, *53*, 3181–3188.
5. Yu, X.; Ye, S. Recent Advances in Activity and Durability Enhancement of Pt/C Catalytic Cathode in PEMFC Part I. Physico-Chemical and Electronic Interaction between Pt and Carbon Support, and Activity Enhancement of Pt/C Catalyst. *J. Power Sources* **2007**, *172*, 133–144.
6. Zignani, S. C.; Antolini, E.; Gonzalez, E. R. Evaluation of the Stability and Durability of Pt and Pt-Co/C Catalysts for Polymer Electrolyte Membrane Fuel Cells. *J. Power Sources* **2008**, *182*, 83–90.
7. Arico, A. S.; Stassi, A.; Modica, E.; Ornelas, R.; Gatto, I.; Passalacqua, E.; Antonucci, V. Performance and Degradation of High Temperature Polymer Electrolyte Fuel Cell Catalysts. *J. Power Sources* **2008**, *178*, 525–536.
8. Beard, K. D.; Schaal, M. T.; Van Zee, J. W.; Monnier, J. R. Preparation of Highly Dispersed PEM Fuel Cell Catalysts Using Electroless Deposition Methods. *Appl. Catal., B* **2007**, *72*, 262–271.
9. Chen, J.-M.; Sarma, L. S.; Chen, C.-H.; Cheng, M.-Y.; Shih, S.-C.; Wang, G.-R.; Liu, D.-G.; Lee, J.-F.; Tang, M.-T.; Hwang, B.-J. Multi-scale Dispersion in Fuel Cell Anode Catalysts: Role of TiO_2 towards Achieving Nanostructured Materials. *J. Power Sources* **2006**, *159*, 29–33.
10. Liu, C.; Xue, X.; Lu, T.; Xing, W. The Preparation of High Activity DMFC Pt/C Electrocatalysts Using a Pre-precipitation Method. *J. Power Sources* **2006**, *161*, 68–73.
11. Min, M.; Park, C.; Kim, H.; Kwak, C.; Serov, A. A.; Kweon, H.; Lee, S. Nano-fabrication and Characterization of New Conceptual Platinum Catalysts for Low Temperature Fuel Cells. *Electrochim. Acta* **2006**, *52*, 1670–1675.
12. Selvaraj, V.; Vinoba, M.; Alagar, M. Electrocatalytic Oxidation of Ethylene Glycol on Pt and Pt−Ru Nanoparticles Modified Multi-walled Carbon Nanotubes. *J. Colloid Interface Sci.* **2008**, *322*, 537–544.
13. Seo, M. H.; Choi, S. M.; Kim, H. J.; Kim, J. H.; Cho, B. K.; Kim, W. B. A Polyoxometalate-Deposited Pt/CNT Electrocatalyst *via* Chemical Synthesis for Methanol Electrooxidation. *J. Power Sources* **2008**, *179*, 81–86.
14. Beard, K. D.; Monnier, J. M.; Van Zee, J. W. Synthesis and Durability of Improved Fuel Cell Catalysts. *Trans. Electrochem. Soc.* **2007**, *2*, 87.
15. Han, K. S.; Moon, Y.-S.; Han, O. H.; Hwang, K. J.; Kim, I.; Kim, H. Heat Treatment and Potential Cycling Effects on Surface Morphology, Particle Size, and Catalytic Activity of Pt/C Catalysts Studied by ^{13}C NMR, TEM, XRD, and CV. *Electrochem. Commun.* **2007**, *9*, 317–324.
16. Kabbabi, A.; Gloaguen, F.; Andolfatto, F.; Durand, R. Particle Size Effect for Oxygen Reduction and Methanol Oxidation on Pt/C Inside a Proton Exchange Membrane. *J. Electroanal. Chem.* **1994**, *373*, 251–254.
17. Kinoshita, K. Particle Size Effects for Oxygen Reduction on Highly Dispersed Platinum in Acid Electrolytes. *J. Electrochem. Soc.* **1990**, *137*, 845–848.
18. Peuckert, M.; Yoneda, T.; Dalla Betta, R. A.; Boudart, M. Oxygen Reduction on Small Supported Platinum Particles. *J. Electrochem. Soc.* **1986**, *133*, 944–947.
19. Schmidt, T. J.; Stamenkovic, V.; Arenz, M.; Markovic, N. M., Jr.; Ross, P. N. Oxygen Electrocatalysis in Alkaline Electrolyte: Pt(*hkl*), Au(*hkl*) and the Effect of Pd-Modification. *Electrochim. Acta* **2002**, *47*, 3765–3776.
20. Takasu, Y.; Ohashi, N.; Zhang, X.-G.; Murakami, Y.; Minagawa, H.; Sato, S.; Yahikozawa, K. Size Effects of Platinum Particles on the Electroreduction of Oxygen. *Electrochim. Acta* **1996**, *41*, 2595–2600.
21. Tian, J. H.; Wang, F. B.; Shan, Z. Q.; Wang, R. J.; Zhang, J. Y. Effect of Preparation Conditions of Pt/C Catalysts on Oxygen Electrode Performance in Proton Exchange Membrane Fuel Cells. *J. Appl. Electrochem.* **2004**, *34*, 461–467.
22. Wikander, K.; Ekstroem, H.; Palmqvist, A. E. C.; Lindbergh, G. on the Influence of Pt Particle Size on the PEMFC Cathode Performance. *Electrochim. Acta* **2007**, 6848–6855.
23. Van Hardeveld, R. Hartog, F. In *Advances in Catalysis*; Eley, D. D., Pines, H., Weisz, P. B., Eds.; Academic Press: New York, 1972; p 75.
24. Luo, J.; Kariuki, N.; Han, L.; Wang, L.; Zhong, C.-J.; He, T. Preparation and Characterization of Carbon-Supported PtVFe Electrocatalysts. *Electrochim. Acta* **2006**, *51*, 4821–4827.
25. Toda, T.; Igarashi, H.; Uchida, H.; Watanabe, M. Enhancement of the Electroreduction of Oxygen on Pt Alloys with Fe, Ni, and Co. *J. Electrochem. Soc.* **1999**, *146*, 3750–3756.
26. Xiong, L.; Kannan, A. M.; Manthiram, A. Pt-M (M = Fe, Co, Ni and Cu) Electrocatalysts Synthesized by an Aqueous Route for Proton Exchange Membrane Fuel Cells. *Electrochem. Commun.* **2002**, *4*, 898–903.
27. Xiong, L.; Manthiram, A. Effect of Atomic Ordering on the Catalytic Activity of Carbon Supported PtM (M = Fe, Co, Ni, And Cu) Alloys for Oxygen Reduction in PEMFCS. *J. Electrochem. Soc.* **2005**, *152*, A697–A703.
28. Antolini, E.; Salgado, J. R. C.; Gonzalez, E. R. Oxygen Reduction on a $Pt_{70}Ni_{30}$/C Electrocatalyst Prepared by the Borohydride Method in H_2SO_4/CH_3OH Solutions. *J. Power Sources* **2006**, *155*, 161–166.
29. Min, M.-k.; Cho, J.; Cho, K.; Kim, H. Particle Size and Alloying Effects of Pt-Based Alloy Catalysts for Fuel Cell Applications. *Electrochim. Acta* **2000**, *45*, 4211–4217.
30. Mukerjee, S.; Srinivasan, S.; Soriaga, M. P.; McBreen, J. Effect of Preparation Conditions of Pt Alloys on Their Electronic, Structural, and Electrocatalytic Activities for Oxygen Reduction: XRD, XAS, and Electrochemical Studies. *J. Phys. Chem.* **1995**, *99*, 4577–4589.
31. Paulus, U. A.; Wokaun, A.; Scherer, G. G.; Schmidt, T. J.; Stamenkovic, V.; Markovic, N. M., Jr.; Ross, P. N. Oxygen Reduction on High Surface Area Pt-Based Alloy Catalysts in Comparison to Well Defined Smooth Bulk Alloy Catalysts. *Electrochim. Acta* **2002**, *47*, 3787–3798.
32. Paulus, U. A.; Wokaun, A.; Scherer, G. G.; Schmidt, T. J.; Stamenkovic, V.; Radmilovic, V.; Markovic, N. M., Jr.; Ross, P. N. Oxygen Reduction on Carbon-Supported Pt−Ni and Pt−Co Alloy Catalysts. *J. Phys. Chem. B* **2002**, *106*, 4181–4191.
33. Stamenkovic, V.; Schmidt, T. J., Jr.; Ross, P. N.; Markovic, N. M. Surface Segregation Effects in Electrocatalysis: Kinetics of Oxygen Reduction Reaction on Polycrystalline Pt_3Ni Alloy Surfaces. *J. Electroanal. Chem.* **2003**, *554−555*, 191–199.
34. Antolini, E.; Salgado, J. R. C.; Giz, M. J.; Gonzalez, E. R. Effects of Geometric and Electronic Factors on ORR Activity of Carbon Supported Pt−Co Electrocatalysts in PEM Fuel Cells. *Int. J. Hydrogen Energy* **2005**, *30*, 1213–1220.
35. Beard, B. C., Jr.; Ross, P. N. the Structure and Activity of Pt−Co Alloys as Oxygen Reduction Electrocatalysts. *J. Electrochem. Soc.* **1990**, *137*, 3368–3374.
36. Salgado, J. R. C.; Antolini, E.; Gonzalez, E. R. Structure and Activity of Carbon-Supported Pt−Co Electrocatalysts for Oxygen Reduction. *J. Phys. Chem. B* **2004**, *108*, 17767–17774.
37. Salgado, J. R. C.; Antolini, E.; Gonzalez, E. R. Carbon Supported $Pt_{70}Co_{30}$ Electrocatalyst Prepared by the Formic Acid Method for the Oxygen Reduction Reaction in Polymer Electrolyte Fuel Cells. *J. Power Sources* **2005**, *141*, 13–18.

38. Santiago, E. I.; Varanda, L. C.; Villullas, H. M. Carbon-Supported Pt−Co Catalysts Prepared by a Modified Polyol Process as Cathodes for PEM Fuel Cells. *J. Phys. Chem. C* **2007**, *111*, 3146–3151.
39. Watanabe, M.; Tsurumi, K.; Mizukami, T.; Nakamura, T.; Stonehart, P. Activity and Stability of Ordered and Disordered Co−Pt Alloys for Phosphoric Acid Fuel Cells. *J. Electrochem. Soc.* **1994**, *141*, 2659–2668.
40. Tseng, C.-J.; Lo, S.-T.; Lo, S.-C.; Chu, P. P. Characterization of Pt−Cu Binary Catalysts for Oxygen Reduction for Fuel Cell Applications. *Mater. Chem. Phys.* **2006**, *100*, 385–390.
41. Antolini, E.; Passos, R. R.; Ticianelli, E. A. Electrocatalysis of Oxygen Reduction on a Carbon Supported Platinum−Vanadium Alloy in Polymer Electrolyte Fuel Cells. *Electrochim. Acta* **2002**, *48*, 263–270.
42. Gattrell, M. MacDougall, B. In *Handbook of Fuel Cells: Fundamentals, Technology and Applications*; Vielstich, W., Gasteiger, H. A., Lamm, A., Eds.; John Wiley & Sons Ltd.: New York, 2003; Vol. 2.
43. Mukerjee, S.; Srinivasan, S.; Soriaga, M. P. Role of Structural and Electronic Properties of Pt and Pt Alloys on Electrocatalysis of Oxygen Reduction. *J. Electrochem. Soc.* **1995**, *142*, 1409–1422.
44. Lima, F. H. B.; Salgado, J. R. C.; Gonzalez, E. R.; Ticianelli, E. A. Electrocatalytic Properties of PtCo/C and PtNi/C Alloys for the Oxygen Reduction Reaction in Alkaline Solution. *J. Electrochem. Soc.* **2007**, *154*, A369–A375.
45. Toda, T.; Igarashi, H.; Watanabe, M. Role of Electronic Property of Pt and Pt Alloys on Electrocatalytic Reduction of Oxygen. *J. Electrochem. Soc.* **1998**, *145*, 4185–4188.
46. Yoshitake, H.; Iwasawa, Y. Electronic Metal-Support Interaction in Pt Catalysts under Deuterium−Ethene Reaction Conditions and the Microscopic Nature of the Active Sites. *J. Phys. Chem.* **1992**, *96*, 1329–1334.
47. Hammer, B.; Norskov, J. K. Theoretical Surface Science and Catalysis—Calculations and Concepts. *Adv. Catal.* **2000**, *45*, 71–129.
48. Hyman, M. P.; Medlin, J. W. Effects of Electronic Structure Modifications on the Adsorption of Oxygen Reduction Reaction Intermediates on Model Pt(111)-Alloy Surfaces. *J. Phys. Chem. C* **2007**, *111*, 17052–17060.
49. Baranton, S.; Coutanceau, C.; Roux, C.; Hahn, F.; Leger, J.-M. Oxygen Reduction Reaction in Acid Medium at Iron Phthalocyanine Dispersed on High Surface Area Carbon Substrate: Tolerance to Methanol, Stability, and Kinetics. *J. Electroanal. Chem.* **2005**, *577*, 223–234.
50. Colon-Mercado, H. R.; Popov, B. N. Stability of Platinum Based Alloy Cathode Catalysts in PEM Fuel Cells. *J. Power Sources* **2006**, *155*, 253–263.
51. He, T.; Kreidler, E.; Xiong, L.; Ding, E. Combinatorial Screening and Nano-Synthesis of Platinum Binary Alloys for Oxygen Electroreduction. *J. Power Sources* **2007**, *165*, 87–91.
52. Adzic, R. R.; Zhang, J.; Sasaki, K.; Vukmirovic, M. B.; Shao, M.; Wang, J. X.; Nilekar, A. U.; Mavrikakis, M.; Valerio, J. A.; Uribe, F. Platinum Monolayer Fuel Cell Electrocatalysts. *Top. Catal.* **2007**, *46*, 249–262.
53. Sasaki, K.; Mo, Y.; Wang, J. X.; Balasubramanian, M.; Uribe, F.; McBreen, J.; Adzic, R. R. Pt Submonolayers on Metal Nanoparticles—Novel Electrocatalysts for H2 Oxidation and O2 Reduction. *Electrochim. Acta* **2003**, *48*, 3841–3849.
54. Sasaki, K.; Wang, J. X.; Balasubramanian, M.; McBreen, J.; Uribe, F.; Adzic, R. R. Ultra-low Platinum Content Fuel Cell Anode Electrocatalysts with a Long-Term Performance Stability. *Electrochim. Acta* **2004**, *49*, 3873–3877.
55. Shao, M.; Sasaki, K.; Marinkovic, N. S.; Zhang, L.; Adzic, R. R. Synthesis and Characterization of Platinum Monolayer Oxygen-Reduction Electrocatalysts with Co−Pd Core−Shell Nanoparticle Supports. *Electrochem. Commun.* **2007**, *9*, 2848–2853.
56. Toshima, N.; Ito, R.; Matsushita, T.; Shiraishi, Y. Trimetallic Nanoparticles Having a Au-Core Structure. *Catal. Today* **2007**, *122*, 239–244.
57. Vukmirovic, M. B.; Zhang, J.; Sasaki, K.; Nilekar, A. U.; Uribe, F.; Mavrikakis, M.; Adzic, R. R. Platinum Monolayer Electrocatalysts for Oxygen Reduction. *Electrochim. Acta* **2007**, *52*, 2257–2263.
58. Wei, Z. D.; Feng, Y. C.; Li, L.; Liao, M. J.; Fu, Y.; Sun, C. X.; Shao, Z. G.; Shen, P. K. Electrochemically Synthesized Cu/Pt Core−Shell Catalysts on a Porous Carbon Electrode for Polymer Electrolyte Membrane Fuel Cells. *J. Power Sources* **2008**, *180*, 84–91.
59. Yao, Y.; Fu, Q.; Zhang, Z.; Zhang, H.; Ma, T.; Tan, D.; Bao, X. Structure Control of Pt−Sn Bimetallic Catalysts Supported on Highly Oriented Pryolytic Graphite (HOPG). *Appl. Surf. Sci.* **2008**, *254*, 3808–3812.
60. Zhang, J.; Vukmirovic, M. B.; Sasaki, K.; Nilekar, A. U.; Mavrikakis, M.; Adzic, R. R. Mixed-Metal Pt Monolayer Electrocatalysts for Enhanced Oxygen Reduction Kinetics. *J. Am. Chem. Soc.* **2005**, *127*, 12480–12481.
61. Zhou, W.; Lee, J. Y. Highly Active Core−Shell Au@Pd Catalyst for Formic Acid Electrooxidation. *Electrochem. Commun.* **2007**, *9*, 1725–1729.
62. Ohno, I. Electrochemistry of Electroless Plating. *Mater. Sci. Eng.* **1991**, *A146*, 33–49.
63. Djokic, S. S. Electroless Deposition of Metals and Alloys. In *Modern Aspects of Electrochemistry*; Conway, B. E., White, R. E., Eds.; Kluwer Academic/Plenum Publishers: Fort Saskatchewan, AB, Canada, 2002; Vol. 35, p 51.
64. Kerr, C.; Barker, D.; Walsh, F. Electroless Deposition of Metals. *Trans. Inst. Met. Finish.* **2001**, *79*, 41–46.
65. Beard, K. D. Ma, S. Van Zee, J. W. Monnier, J. R. XPS Study of Pt−Pd Bimetallic Catalysts Prepared by Electroless Deposition *Langmuir*, submitted for publication.
66. Beard, K. D.; Van Zee, J. W.; Monnier, J. R. Preparation of Carbon-Supported Pt Electrocatalysts Having Improved Physical Properties Using Electroless Deposition Methods. *Appl. Catal., B* **2008**, 185–193.
67. Schaal, M. T.; Metcalf, A. Y.; Montoya, J. H.; Wilkinson, J. P.; Stork, C. C.; Williams, C. T.; Monnier, J. R. Hydrogenation of 3,4-Epoxy-1-butene over Cu−Pd/SiO_2 Catalysts Prepared by Electroless Deposition. *Catal. Today* **2007**, *123*, 142–150.
68. Schaal, M. T.; Pickerell, A. C.; Williams, C. T.; Monnier, J. R. Characterization and Evaluation of Ag−Pt/SiO_2 Catalysts Prepared by Electroless Deposition. *J. Catal.* **2008**, *254*, 131–143.
69. Brotons, V.; Coq, B.; Planeix, J. M. Catalytic Influence of Bimetallic Phases for the Synthesis of Single-Walled Carbon Nanotubes. *J. Mol. Catal. A* **1997**, *116*, 397–403.
70. Niemelae, M. K.; Krause, A. O. I.; Vaara, T.; Kiviahol, J. J.; Reinikainen, M. K. O. The Effect of the Precursor on the Characteristics of Co/SiO_2 Catalysts. *Appl. Catal., A* **1996**, 325–345.
71. Reinikainen, M.; Niemela, M. K.; Kakuta, N.; Suhonen, S. Characterisation and Activity Evaluation of Silica Supported Cobalt and Ruthenium Catalysts. *Appl. Catal., A* **1998**, *174*, 61–75.
72. Schanke, D.; Vada, S.; Blekkan, E. A.; Hilmen, A. M.; Hoff, A. Study of Pt-Promoted Cobalt CO Hydrogenation Catalysts. *J. Catal.* **1995**, *156*, 85–95.
73. Thormaehlen, P.; Skoglundh, M.; Fridell, E.; Andersson, B. Low-Temperature CO Oxidation of Platinum and Cobalt Oxide Catalysts. *J. Catal.* **1999**, *188*, 300–310.
74. Lelental, M. Dimethylamine Borane as the Reducing Agent in Electroless Plating Systems. *J. Electrochem. Soc.* **1973**, *120*, 1650–1654.
75. Lelental, M. Effect of Amine Borane Structure on Activity in Electroless Plating. *J. Catal.* **1974**, *32*, 429–433.
76. Bulou, H.; Barbier, A.; Belkhou, R.; Guillot, C.; Carriere, B.; Deville, J. P. Chemical Structure of the Pt/Co(0001) Interface. *Surf. Sci.* **1996**, *352−354*, 828–832.
77. Cabeza, G. F.; Legare, P.; Sadki, A.; Castellani, N. J. Growth and Structure of Thin Platinum Films Deposited on Co(0001) Studied by Low-Energy Electron Diffraction, X-ray Photoelectron Spectroscopy, Ultraviolet Photoelectron Spectroscopy and Scanning Tunneling Microscopy. *Surf. Sci.* **2000**, *457*, 121–133.

78. Pattanaik, G.; Kirkwood, D. M.; Xu, X.; Zangari, G. Electrodeposition of Hard Magnetic Films and Microstructures. *Electrochim. Acta* **2007**, *52*, 2755–2764.
79. Sahari, A.; Azizi, A.; Fenineche, N.; Schmerber, G.; Dinia, A. Electrochemical Study of Cobalt Nucleation Mechanisms on Different Metallic Substrates. *Mater. Chem. Phys.* **2008**, *108*, 345–352.
80. Beard, K. D. Ph.D Dissertation, University of South Carolina, 2009.
81. Pirjamali, M.; Kiros, Y. Effects of Carbon Pretreatment for Oxygen Reduction in Alkaline Electrolyte. *J. Power Sources* **2002**, *109*, 446–451.